Strength size effect in quasi-brittle structures

B. L. Karihaloo, Q. Z. Xiao and H. M. Abdalla
School of Engineering, Cardiff University, Queen's Buildings, P O Box 925, Cardiff, CF24 0YF, UK

ABSTRACT: Quasi-brittle materials are usually heterogeneous and are characterised by the prersence of a large fracture process zone (FPZ) where much of the energy supplied by external sources is dissipated before any real crack proporgation can take place. For their description it is therefore essential to know how the energy is dissipated and how the stresses are redistributed in the FPZ. This in turn is dependent on the microstructure of the material. Thus the coarser the microstructure the larger the extent of FPZ, and vice versa. Current test procedures produce results which show a marked dependence of the specific fracture energy on the shape and size of the test specimen because of specimen boundary effects which make the energy dissipation non-uniform in the FPZ. The authors have recently shown how to take this boundary effect into account in order to obtain a size-independent specific fracture energy of a quasi-brittle material, and the corresponding tension-softening diagram.

The failure strength of structures made from quasi-brittle materials seems to decrease as the size of the structure is increased. This apparent size effect is claimed not to be of the statistical nature but as a result of high stress gradients introduced by cracks. In this paper it will be shown that this claim is strictly true for cracks of moderate size relative to the size of structure. For very small cracks (again relative to the structural size) the strength size effect is only slightly different from the Weibull statistical size effect. A theoretical explanation of strength size effect will be provided over the size range 1:80. It is interesting to point out that this explanation needs the above-mentioned size-independent specific fracture energy and the corresponding tension-softening relationship.

The computational results have been fitted by a simple strength size effect formula with appropriate asymptotic behaviour at both size extremes. The three unknown coefficients in this formula depend only on the size of the crack and they can be obtained by conducting tests on geometrically similar specimens of any shape but of varying sizes that can be conveniently handled in a laboratory. The three material properties of the concrete mix appearing in this formula, namely the Young modulus E, the direct tensile strength f_t and the size-independent specific fracture energy G_F must be independently measured.

Keywords: quasi-brittle material, size effect, specific fracture energy, tension-softening

1. INTRODUCTION

In quasi-brittle materials, any crack or notch tips are blunted by the formation of a process zone ahead them. In this process zone the stresses are redistributed and energy dissipated which is thus not available for crack propagation. The size of this fracture process zone (FPZ) can be commensurate with that of most structural elements. Only in very large structures can this size be regarded as small in comparison with the characteristic dimensions.

The redistribution of stresses and dissipation of energy in the FPZ was accounted for by Bazant (1984) who derived the formula

$$(\sigma_N)_u = \frac{A_2}{(1+W/B_2)^{\frac{1}{2}}} \tag{1}$$

where A_2 and B_2 are positive coefficients. Formula (1) reduces to the linear elastic fracture mechanics as $W \to \infty$ when the size of the FPZ is very small in comparison with W. In fact formula (1) can be established by Taylor's expansion from this asymptotic limit (Karihaloo 1995). Since its appearance in the literature in 1984, formula (1) has been rederived from energy considerations and asymptotic matching techniques (see, e.g. Bazant 1997, Bazant & Chen 1997). The positive coefficients A_2 and B_2 are related to the specific fracture energy G_f and the FPZ size c_f measured on a very large specimen ($W \to \infty$), as well as the non-dimensional geometry factor g(α) and its first derivative g′(α). The geometry factor g(α) depends on the notch to depth ratio $\alpha = a/W$ and is different for different test specimen shapes

$$A_2 = \left(\frac{EG_f}{g'(\alpha) c_f} \right)^{\frac{1}{2}} \quad ; \quad B_2 = c_f \frac{g'(\alpha)}{g(\alpha)} \tag{2}$$

It has been argued that the relationships between the coefficients A_2 and B_2 and the material properties G_f and c_f (2) can be exploited to determine the latter from tests on notched specimens of various sizes with two-dimensional similarity. For example, tests can be conducted on notched three-point bend (TPB) beams with a fixed α and span to depth ratio for several depth values. The coefficients A_2 and B_2 are determined by a linear regression analysis, after rewriting (1) in the standard form $Y = AX + B$, where

$Y = 1/(\sigma_N)_u^2$, $X = W$, $A = 1/(B_2 A_2^2)$ and $B = 1/A_2^2$.

Another approach to capturing the FPZ within a nonlinear theory of fracture for quasi-brittle materials is the so-called fictitious crack model (FCM) of Hillerborg et al. (1976). In this model, the FPZ ahead of a real crack is replaced with a fictitious crack in which the material exhibits softening with a residual stress transfer capability across the crack faces dependent on the crack opening displacement (COD), $\sigma(w)$. The faces of the fictitious crack are assumed to close smoothly near the tips so that the stress is finite at the fictitious crack tip and equal to the tensile strength f_t of the quasi-brittle material. Thus the net stress intensity factor (SIF) (i.e. the SIF due to external loading less the factor due to the closure pressure in the FPZ) vanishes at the fictitious crack tip.

This approach was adopted by Karihaloo (1999) who arrived at the formula

$$(\sigma_N)_u = A_3 \left(1 - \frac{B_3}{W} \right)^{\frac{1}{2}} \tag{3}$$

where

$$A_3 = (\sigma_N)_{u\infty}, \; B_3 = \frac{1}{2} l_{p\infty} \frac{g'(\alpha)}{g(\alpha)} \tag{4}$$

Here, $l_{p\infty}$ and $(\sigma_N)_{u\infty}$ refer to the size of the FPZ in a very large specimen ($W \to \infty$) and its nominal strength. It was argued by Karihaloo (1999) that $l_{p\infty}$ and $(\sigma_N)_{u\infty}$ can be obtained by considering only the singular term of the stress field ahead of a pre-existing crack, whereas for normal size structures higher order terms need to be considered to take into account the relatively large size of the FPZ in the FCM.

In the derivation of formula (3) several approximations and assumptions were made, as a result of which its predictions for small values of W were suspect. This was pointed out by Planas et al. (2001) and by Karihaloo et al. (2003b). The latter authors also made a tentative attempt at dispensing with some of the approximations and assumptions in its derivations. Apart from these drawbacks, it is not clear how the asymptotic properties G_f and $l_{p\infty}$ can be used for the analysis of real structures. Moreover, it transpires that both G_f and $l_{p\infty}$ (or c_f in formula (1)) cannot be regarded as material properties because they vary with α, W and the shape of the test specimen. That brings us to the essential question that we shall attempt to answer in this paper. How much of the size effect in the strength of a quasi-brittle structure predicted by formula (3) (or formula (1)) is a result of the intrinsic size effect in the G_f itself? In other words, if the specific fracture energy of a quasi-brittle material that did not depend on the shape and size of the test specimen could be independently determined, would a structure made of such a material still exhibit a strong size effect in strength?

In this paper we shall revisit the formulation of formula (3) with a view to predicting the observed nominal strengths of TPB and wedge splitting (WS) specimens made from normal and high strength concretes. Both these specimen geometries belong to the so-called type 2 geometry, i.e. g (α) > 0, g′(α) > 0. We shall propose an improved formula for predicting the strength size effect over a large size range of 1:80.

2. TEST RESULTS, G_F AND $\sigma(W)$

Tests were conducted on TPB and WS specimens (for full details, see Abdalla & Karihaloo 2003). Notched beams of different depths W (100, 200, 300 and 400 mm) with a constant span to depth ratio of 4 were tested in three point bending (Fig.

1). The notch to depth ratios a/W were selected to be 0.05, 0.10, 0.30 and 0.50.

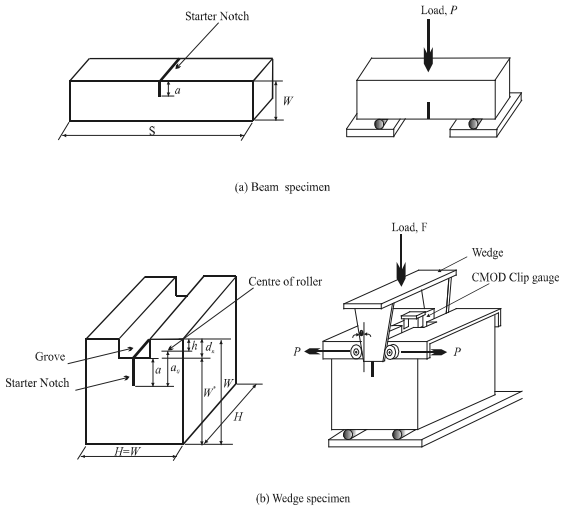

Figure 1. Specimen shapes, dimensions and loading arrangements (a) beam specimen; (b) wedge specimen.

WS tests were carried out on normal and high strength concretes. Their average compressive strengths were 60 and 100 MPa, respectively. Ninety-six specimens of different sizes W (100, 200 and 300 mm) were tested (Fig. 1). The notch to depth ratios $a_0/(W-h)$ were selected to be 0.20, 0.30, 0.40 and 0.50 (the corresponding a/W^* ratios are 0.16, 0.26, 0.36 and 0.46, see Fig. 1).

The value of the specific fracture energy so determined varies with the size and the notch to depth ratio α. This value is therefore designated $G_f(\alpha, W)$. It decreases with increasing α but increases with increasing W (for details, see Abdalla & Karihaloo 2003).

Table 1. Size-independent specific fracture energy G_F.

TPB specimens of NSC (55 MPa)	W mm	100	200	300	400
	G_F N/m	140	144	137	143
	a_l mm	54	104	117	149
WS specimens NSC (60 MPa)	W mm	100	200	300	
	G_F N/m	153	155	156	
	a_l mm	79	136	166	
HSC (100 MPa)	G_F N/m	125	122	123	
	a_l mm	74	128	187	

The application of the boundary effect concept (Duan et al. 2003) to the test results $G_f(\alpha, W)$ indeed gives a specific fracture energy value G_F that is independent of the size (α, W) and shape of the test specimen. This may be judged by the values reported in Table 1.

For both the TPB and WS specimens the size-independent specific fracture energy G_F (Table 1) was estimated from three or four sizes with four notch to depth ratios. However, Abdalla & Karihaloo (2003) also observed that the same value of G_F for a concrete mix could also be obtained by testing specimens of a single size, one half of them containing a very shallow starter crack ($\alpha \le 0.10$ for TPB and $\alpha \le 0.16$ for WS) and the other half a deep starter crack ($\alpha \ge 0.50$ for TPB and WS). This observation was confirmed recently (Karihaloo et al., 2003a) by re-evaluation of a large body of test data on measured $G_f(\alpha, W)$ of concrete mixes available in the literature. This conformation paved a way for a simple and practical means of determining G_F of concrete. They also provided guidance for the selection of the specimen dimensions based on the maximum size of aggregate in the concrete mix.

In the context of the FCM (Hillerborg et al. 1976) the true specific fracture energy obtained above is exactly equal to the area under the cohesive stress-separation diagram $\sigma(w)$ (i.e. the tension softening diagram) in the fictitious crack (i.e. the FPZ)

$$G_F = \int_0^{w_c} \sigma(w)\, dw \tag{5}$$

where w_c is the critical opening of the real crack tip when it begins to grow.

As the tension softening region (i.e. the fictitious crack) is generally discontinuous, a direct determination of $\sigma(w)$ is an impossible task. It is therefore often determined using an inverse identification procedure. Many such procedures have been proposed (Roelfstra & Wittmann 1986, Ulfkjaer et al. 1995, Olesen 2001). In each of these procedures, the shape of the tension softening diagram is assumed *a priori* and the parameters describing it identified in such a way that the global load-deformation response of the test specimen is reproduced with a desired degree of accuracy. By far the most popular approximation of the $\sigma(w)$ diagram is the bilinear one shown in Fig. 2, so that (5) reduces to

$$G_F = \frac{1}{2}\left(f_t w_1 + f_1 w_c\right) \tag{6}$$

where w_1, f_1 and w_c are to be identified. In this work, the simple inverse identification procedure of Olesen (2001) based on a nonlinear hinge model for the real and fictitious crack was used to identify these three parameters for the three concrete mixes tested using the TPB and WS specimens. The

global load-CMOD response of the specimens was reproduced for all W and α. The average values of the parameters w_1, f_1 and w_c were scaled to correspond to the size-independent G_F of concrete mixes (Table 1). The resulting parameters of the bilinear $\sigma(w)$ diagram for the three mixes are given in Table 2.

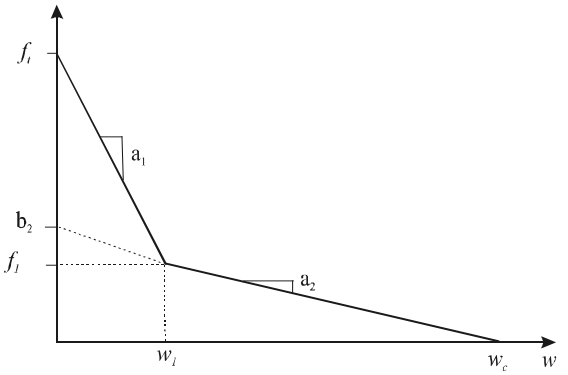

Figure 2. Bilinear tension softening diagram $\sigma(w)$.

Table 2. Elastic properties and parameters of $\sigma(w)$ diagram for the three test concrete mixes.

Mix	f_c (MPa)	f_t (MPa)	G_F (N/m)	E (GPa)	w_1 (mm)	f_1 (MPa)	w_c (mm)	l_{ch} (mm)
NSC for TPB	55	2.67	141	36.9	0.049	0.457	0.333	729.8
NSC for WS	60	2.80	155	38.3	0.051	0.524	0.318	757.2
HSC for WS	100	4.00	123	43.0	0.017	1.36	0.132	330.6

The direct tensile strength was assumed to be f_t = 0.65 f_{st}, where f_{st} is the indirect tensile strength, namely the split cylinder strength.

3. THEORETICAL PREDICTIONS

In the derivation of formula (3) (Karihaloo 1999) it was recognised that quasi-brittle materials develop a diffuse FPZ before the formation of a traction-free crack whose size can be commensurate with that of a small test specimen. Within this zone the stresses are redistributed so that it is necessary to consider not only the singular term in the asymptotic crack tip field but also higher order, nonsingular terms. In the derivation, Karihaloo (1999) used approximations for the higher order terms, as well as the weight (Green's) functions for a semi-infinite crack in an infinite plane instead of a finite size crack in a finite TPB or WS specimen. These approximations have now been eliminated by taking into account accurate higher order terms of the crack tip asymptotic field, as well as by using accurate weight functions for a finite crack. Some preliminary results have been previously reported (Karihaloo et al. 2003b).

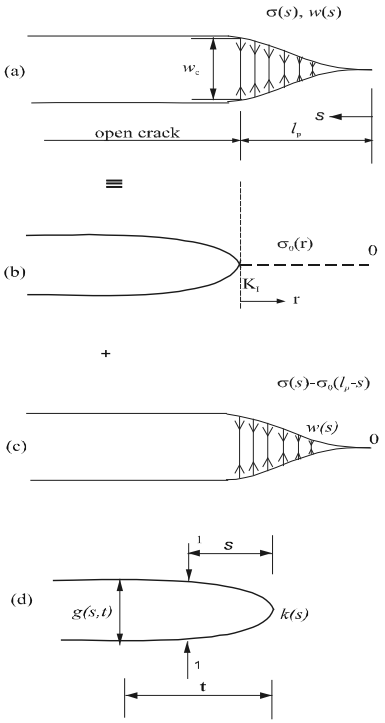

Figure 3. Decomposition of a traction free crack with a FPZ of length l_p (a) into the traction free crack with stress σ_0 (r) ahead of crack tip (b) and the FPZ with stress [$\sigma(s)$ - $\sigma_0(l_p - s)$] and displacement w(s)(c). As the faces close smoothly the stress intensity factor at *0* will vanish. k(s) is the stress intensity factor due to unit concentrate loads at s, $g(s, t)$ is the corresponding displacement at location t (d) (From Karihaloo 1995).

In common with the earlier derivation (Karihaloo 1999), the traction-free crack with a FPZ of length l_p at its tip is decomposed into a traction-free crack (Fig. 3) with the following stress field at its tip

$$\sigma_y(r) \equiv \sigma_0(r) = \frac{a_1}{\sqrt{r}} + 3a_3\sqrt{r} + 5a_5 r^{\frac{3}{2}} \qquad (7)$$

and the FPZ with the stress [$\sigma(s)$ - $\sigma_0(l_p$-$s)$] and the displacement $w(s)$ across its faces. In (7), a_1 is related to the mode I SIF K_I via a_1 = K_I / $\sqrt{(2\pi)}$. The coefficients a_1, a_3 and a_5 depend on the crack length, applied load σ and size and geometry of the body.

For a TPB with a span to depth ratio β of 4 considered in the current study, the coefficients a_1, a_3, a_5 are (Karihaloo & Xiao 2001)

$$a_1 = \sigma\sqrt{W}\, k_4(\alpha)$$
$$a_3 = \frac{\sigma}{\sqrt{W}}\, g_4^3(\alpha) \qquad (8)$$

$$a_5 = \frac{\sigma}{W^{3/2}}\ g_4^5(\alpha)$$

where

$$k_4(\alpha) = \frac{\sqrt{\alpha}\ p_4(\alpha)}{\sqrt{2\pi}\ (1-\alpha)^{3/2}\ (1+3\alpha)}$$

$$p_4(\alpha) = 1.9 + 0.41\alpha + 0.51\alpha^2 - 0.17\alpha^3$$

$$g_4^3(\alpha) = -148.73\alpha^5 + 233.48\alpha^4 - 153.97\alpha^3 + 49.515\alpha^2 - 9.2406\alpha + 0.6534 \quad (9)$$

$$g_4^5(\alpha) = 2765.2\alpha^6 - 5869.4\alpha^5 + 4919.3\alpha^4 - 2084.4\alpha^3 + 468.48\alpha^2 - 52.998\alpha + 2.1491$$

and $\sigma = 6P/W$ and the subscript 4 refers to the span to depth ratio $\beta = 4$. P is the applied point load per unit thickness (m). The dimensions of σ and W are MPa and m, respectively. For brevity, we shall not report the theoretical/computational results for WS geometry.

The opening displacement of the cohesive crack faces $w(t)$ (representing the FPZ) can be expressed as the following singular integral equation (see Fig. 3)

$$\int_0^{l_p} g(s,t;a)\left[\sigma(s) - \sigma_0\left(l_p - s\right)\right]ds = -w(t) \quad (10)$$

The finite tensile strength of concrete requires that SIF vanishes at the FPZ tip. This in turn requires that the faces of FPZ close smoothly, i.e.

$$\int_0^{l_p} k(s;a)\left[\sigma(s) - \sigma_0\left(l_p - s\right)\right]ds = 0 \quad (11)$$

Of course, it is not always necessary to impose the condition that the SIF vanishes at the FPZ tip (see e.g. Elices et al. 2002). In normal strength concrete, the FPZ is often surrounded by a zone of microcracks (corresponding to the pre-peak nonlinearity), so that the SIF is finite at the FPZ tip. However, this has been shown to have a negligible effect on the results (Alaee & Karihaloo 2003).

The weight functions $g(s,t;a)$ and $k(s;a)$ are the respective COD at the location t and the SIF at the crack tip of a single edge cracked specimen of finite size due to a pair of unit normal forces at s on the crack faces (Fig. 3d). Both $k(s;a)$ and $g(s,t;a)$ have been derived by Xiao & Karihaloo (2002).

In the earlier formulation leading to eqn (3) (Karihaloo 1999) the following crucial approximations were made: (i) the higher order coefficient a_3 was inferred indirectly and a_5 was not included; (ii) only the first terms in the weight functions (10) and (11) were used. These terms correspond to a semi-infinite crack in an infinite body and not the finite TPB or WS specimens considered; (iii) with these approximations, the two singular integral equations (10) and (11) were solved analytically in an indirect manner. The COD, $w(s)$, in the FPZ $0 \le s \le l_p$ was approximated by a polynomial in s, and $\sigma(s)$ and l_p were solved analytically from (10) and (11) for prescribed σ (i.e. K_I). The distance s was then eliminated from the assumed $w(s)$ and the calculated $\sigma(s)$ to establish the tension softening relationship $\sigma(w)$.

As a result of the above approximations, the $\sigma(w)$ relationship so obtained became dependent on the geometry of the structure and external loading (i.e. on σ and a_3) and no longer reflected a true material property, as it should. Additionally, the nominal strength formula (3) predicted an arbitrary lower limit on the structural size $W > B_3$ in order for it to have a physical meaning.

The above exact formulation has overcome these drawbacks. However, it is now necessary to prescribe the actual $\sigma(w)$ diagram for the concrete used for making the TPB beams and WS specimens and to solve the singular integral equations (10) and (11) numerically for the prescribed $\sigma(w)$ diagram (Table 2).

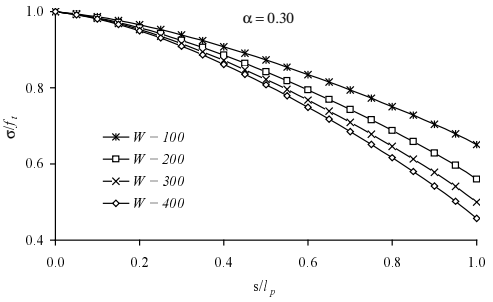

Figure 4. Distribution of the cohesive stress in the FPZ for TPB specimens with $\alpha = 0.30$ and various W.

To solve the singular integral equations (10) and (11), the FPZ is divided into segments as is usually done in the boundary element analysis. The cohesive stress $\sigma(s)$ is interpolated by its values at the two end points and assumed to vary linearly within each segment. Equation (10) is discretized at all nodes except the FPZ tip, where the value of cohesive stress equals f_t. From the discretized system of equations, we can solve the unknown cohesive stresses and external applied stress σ (or l_p) for given l_p (or σ). The typical distribution of the cohesive stress in the FPZ at peak load is

shown in Fig. 4, for TPB specimens with $\alpha = 0.30$ and various W values. The distributions are very similar for all values of α, and for all α and W, the residual stress is always above the level of f_1 (Table 2).

4. DISCUSSION

It can be seen that when the crucial simplifying assumptions made in the derivation of formula (3) are removed, the predictions of the resulting formulation based on the FCM are in good agreement with the test results for TPB specimens (Fig. 5). (The same procedure can be followed for WS specimens. However, for brevity, calculations for WS specimens are not included here). This good agreement is a result of using G_F and $\sigma(w)$ in the FCM that are independent of the shape and size of the test specimen (Tables 1 and 2).

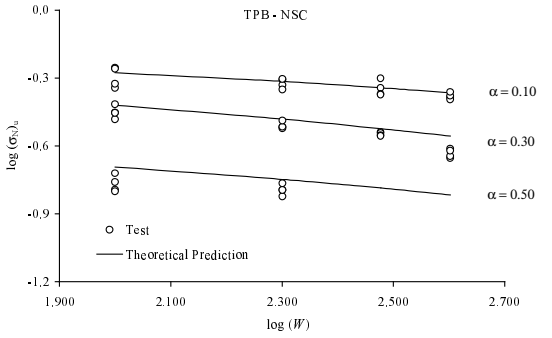

Figure 5. The variation of the measured nominal strength with the characteristic dimension, W of the TPB specimen compared with the theoretical prediction.

It is of some interest to study the weakening in the strength size effect as the size of the notch decreases with a view to judging whether or not there is a deterministic fracture mechanical size effect (over and above the statistical Weibull size effect) in unnotched quasi-brittle structures. For this the test results for the TPB specimens with a very small initial notch ($\alpha = 0.05$) are again plotted in Fig. 6 on a log-log scale, together with the Weibull line which on the same scale has a slope close to –1/6 (Zech & Wittmann 1978). Note that it is not possible to test WS specimens with very small α (smaller than around $\alpha = 0.15$) because they tend to fail prematurely at the re-entrant corners (Fig. 1). From Fig. 6 it is clear that there is a (small) size effect in the failure strength over and above the statistical Weibull size effect, but it is difficult to say with any degree of certainty as to whether this small difference is solely due to the deterministic fracture mechanical size effect. This is because casting and curing of concrete specimens induce their own size effects. Van Vliet & Van Mier (1999) also noticed that uniaxial tension test strength data on unnotched specimens could be accurately described by Weibull statistics (apart from the very small test specimen) but cautioned against drawing any definitive conclusions on strength size effect from this fortuitous agreement because of the size effects induced by casting and curing of specimens.

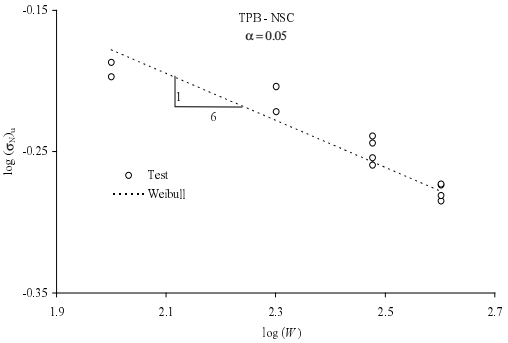

Figure 6. The variation of the measured nominal strength of TPB specimen with a very small starter notch ($\alpha = 0.05$) with the specimen depth W compared with the Weibull statistical size effect for concrete.

In view of the fact that the theoretical model based on the FCM and the use of size-independent G_F and $\sigma(w)$ of a concrete mix is able to predict the strength size effect accurately in the range of sizes of TPB specimens tested in the laboratory, the model has been used to predict the nominal failure strength outside of this range. The size of TPB beams, made from the same normal strength concrete mix from which the test beams were made, was varied between W = 25mm and W = 2000mm keeping the span to depth ratio constant at 4. This gave a size range of 1:80. Three notch to depth ratios were considered, $\alpha = 0.1$, 0.3 and 0.5. The results of this prediction are shown in Fig. 7, together with the test results. The relative size of the FPZ (l_p/W) is shown in Fig. 8 from which it is clear that l_p/W decreases significantly as W increases. For example, it drops from 0.64 to 0.107, as W increases from 25 to 2000mm for $\alpha = 0.10$. This confirms conclusively that nonlinear theory of fracture is essential for structures of small size but that large concrete structures with cracks can be analysed by linear elastic fracture theory.

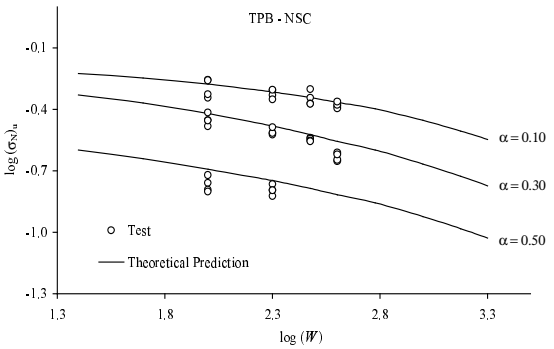

Figure 7. The variation of the nominal strength with the characteristic dimension, W of the TPB geometry as predicted by the theoretical model in the extended size range from 25 to 2000mm.

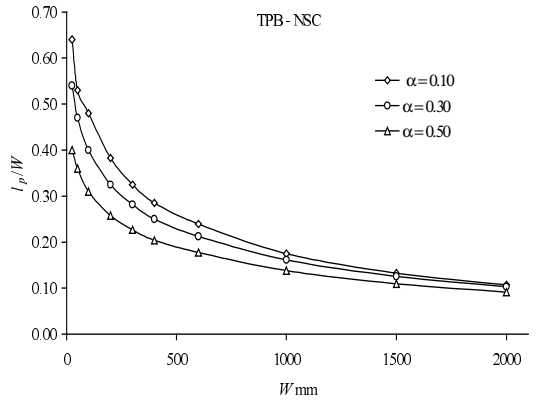

Figure 8. The variation of the relative size of the FPZ with the characteristic dimension, W of the TPB geometry for the size range from 25 to 2000mm.

5. IMPROVED FORMULA (3)

We have seen above that the theoretical model based on the FCM is able to predict accurately not only the test results in the narrow range of sizes tested in the laboratory but also outside of it (Fig. 7). However, these predictions are only available to those who can perform the computations. For this reason, it would be most helpful to have the computational results available in a simple analytical form, as e.g. formula (3) but without its drawbacks. This analytical formula would replace the inadequate (3).

With this aim in mind, we shall assume, based on the expected asymptotic behaviour that

$$\frac{(\sigma_N)_u}{f_t} = \frac{D_1}{\left(1+\frac{W/l_{ch}}{D_2}\right)^{\frac{1}{2}}} + \frac{D_3}{\left(1+\frac{D_4}{W/l_{ch}}\right)} \tag{12}$$

where, $D_1,\ldots, D_4$ are coefficients to be determined by fitting the test results.

The choice of (12) is dictated by the fact that the strength attains finite asymptotic values at both size extremes, i.e. when $W \to 0$ and $W \to \infty$. However, for $(\sigma_N)_u$ to tend to a finite value as $W \to 0$, we must have additionally that $d(\sigma_N)_u/dW \to 0$ as $W \to 0$. For this it is necessary and sufficient that

$$D_3 = \frac{D_1 D_4}{2D_2} \tag{13}$$

As $D_1 > D_3$, it follows from (13) that

$$D_4/D_2 < 2 \tag{14}$$

Equation (12) can therefore be rewritten as

$$\frac{(\sigma_N)_u}{f_t} = D_1(\alpha)\left(1+\frac{W/l_{ch}}{D_2(\alpha)}\right)^{-\frac{1}{2}} + \frac{D_1(\alpha)}{2D_2(\alpha)}\,\frac{W}{l_{ch}}\left(1+\frac{W/l_{ch}}{D_4(\alpha)}\right)^{-1} \tag{15}$$

The coefficients $D_1(\alpha)$, $D_2(\alpha)$ and $D_4(\alpha)$ are obtained by nonlinear regression of the test results and are given in Table 3, together with $D_3(\alpha)$ obtained using eqn (13). Note that the inequality (14) is satisfied for all α and all three mixes.

Table 3. Coefficients $D_1,\ldots..,\ D_4$ in (12) and (15) for the three concrete mixes.

Mix	f_c (MPa)	α	$D_1(\alpha)$	$D_2(\alpha)$	$D_4(\alpha)$	$D_3(\alpha)$ (eqn (13))
NC for TPB	55	0.05	0.263	0.493	0.081	0.022
		0.10	0.211	0.481	0.001	0.0003
		0.30	0.156	0.254	0.029	0.009
		0.50	0.066	0.371	0.194	0.007
NC for WS	60	0.16	0.161	0.084	0.055	0.053
		0.26	0.177	0.013	0.088	0.054
		0.36	0.090	0.029	0.026	0.040
		0.46	0.051	0.407	0.079	0.005
HSC for WS	100	0.16	0.177	1.412	0.382	0.024
		0.26	0.158	0.401	0.109	0.021
		0.36	0.096	0.901	0.054	0.003
		0.46	0.104	0.064	0.024	0.020

The formula (15) is plotted on Figs 9-11 for the three concrete mixes, together with formula (1). It will be seen that eqn (15) fits the experimental data well. The predictions of the size effect formula (1) are also in good agreement with the test results. However, when the relationships (2) between the coefficients A_2 and B_2 appearing in this formula and the material properties G_f and c_f are exploited, the resulting material properties are found to vary

significantly with the shape and size of the test specimen.

Equation (15) does have the correct asymptotic behaviour, although the coefficients $D_1(\alpha)$, $D_2(\alpha)$ and $D_4(\alpha)$ were determined from test data in a limited size range. In order to check whether or not it can be used outside of this narrow range, we shall compare its prediction with those of the theoretical/computational model (Fig. 7) for the NSC using TPB geometry for α = 0.10, 0.30 and 0.50.

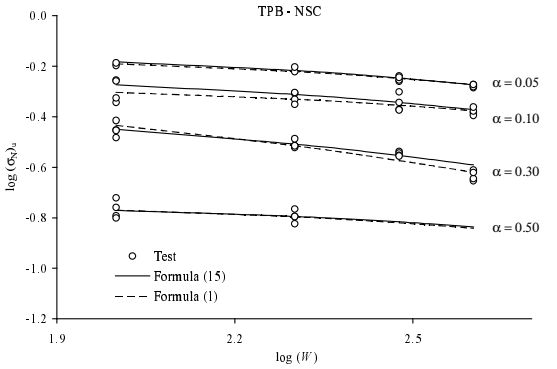

Figure 9. The variation of the measured nominal strength with the characteristic dimension, W of the TPB specimen compared with formula (15) and formula (1).

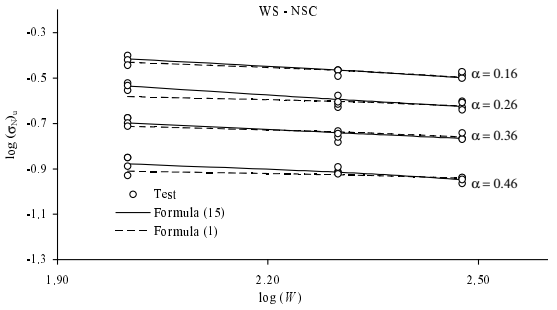

Figure 10. The variation of the measured nominal strength with the characteristic dimension, W of the WS specimen for NSC compared with formula (15) and formula (1).

The comparison of predictions is shown in Fig. 12, from which it is clear that formula (15) can indeed be used in the size range 1:80 for shallow to moderate notches. The theoretical/computational predictions deviate from those of formula (15) for α = 0.50. However, we believe this is a result of the fact that the test results were only available for two depths for this ratio of notch to depth.

Formula (15) therefore replaces the inadequate formula (3). The coefficients in this formula are established from specimens of a range of sizes and a range of notch to depth ratios that can be conveniently tested in a laboratory. The formula can then be used in a much larger size range (1:80) with confidence.

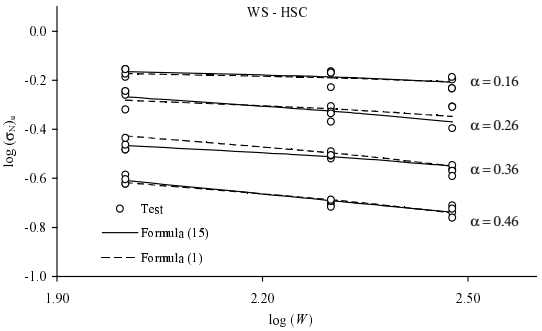

Figure 11. The variation of the measured nominal strength with the characteristic dimension, W of the WS specimen for HSC compared with formula (15) and formula (1).

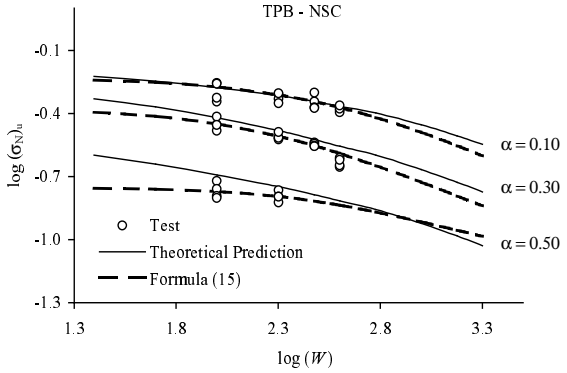

Figure 12. Comparison of theoretical/computational predictions with those of formula (15) in the size range 1:80.

As a matter of interest, we have plotted formula (15) in a still larger size range (1:10^6) in Fig. 13 of TPB geometry for two notch to depth ratios, together with the test results. The formula seems to capture the whole range accurately.

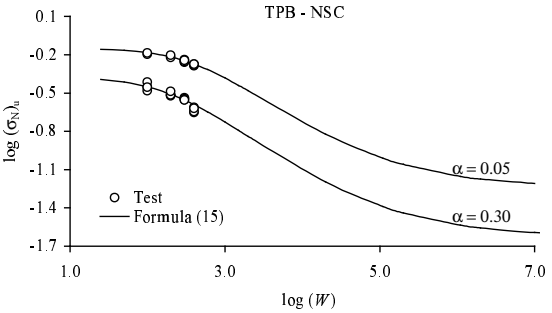

Figure 13. Prediction of formula (15) over the size range 1:10^6. The test data in the narrow size range are also shown (α = 0.05 and 0.30).

6. CONCLUSIONS

Based on the work reported in this paper, the following conclusions can be drawn.

- A deterministic (as opposed to statistical) size effect exists in the strength of cracked concrete structures owing to the stress redistribution introduced by the presence of cracks manifested in the FPZ.
- The deterministic strength size effect becomes stronger as the size of the cracked structure increases but weakens as the size of the crack reduces relative to the size of the structure. These experimental observations are confirmed by theoretical/computational studies based on the FCM. For these studies it is important however to use the true, size-independent fracture energy and the corresponding tension softening diagram of the concrete mix that are independently measured.
- The theoretical/computational model that is in full agreement with the test results in the limited range of sizes tested in the laboratory can be extended beyond this range to include cracked concrete structures in the very large size range of 1:80.
- The theoretical/computational results in this extended size range can be represented by a strength size effect formula that is very simple to use in practice and has the appropriate asymptotic behaviour of both size extremes.
- Besides the mix properties (Young's modulus, E, direct tensile strength, f_t, and the true size-independent specific fracture energy, G_F) which must be independently measured, this simple formula contains three unknown coefficients which depend only on the size of the crack relative to the size of the structure (i.e. α).
- These three coefficients can be determined by regression on test results obtained on geometrically similar specimens of any shape but of varying sizes and α that can be conveniently handled in a laboratory. The formula can be used with confidence for cracked concrete structures in the range of at least 1:80.

REFERENCES

Abdalla, H.M. & Karihaloo, B.L. 2003. Determination of size-independent specific fracture energy of concrete from three-point bend and wedge splitting tests. *Mag Concr Res* 55: 133-141.

Alaee, F.J. & Karihaloo, B.L. 2003. A fracture model for flexural failure of beams retrofitted with CARDIFRC®. *ASCE J Engng Mech* 129: 1028-1038.

Bazant, Z.P. 1984. Size effect in blunt fracture: concrete, rock, metal. *ASCE J Engng Mech* 110: 518-535.

Bazant, Z.P. 1997. Scaling of quasi-brittle fracture: asymptotic analysis. *Int J Fract* 83: 19-40.

Bazant, Z.P. & Chen, E.P. 1997. Scaling of structural failure. *Appl Mech Rev* 50: 593-627.

Duan, K., Hu, X.Z. & Wittmann, F.H. 2003. Boundary effect on concrete fracture and non-constant fracture energy distribution. *Engng Fract Mech* 70: 2257-2268.

Elices, M., Guinea, G.V., Gómez, J. & Planas, J. 2002. The cohesive zone model: advantages, limitations and challenges. *Engng Fract Mech* 69:137-163.

Hillerborg, A., Modéer, M. & Petersson, P.E. 1976. Analysis of crack formation and crack growth in concrete by means of fracture mechanics and finite elements. *Cement Concr Res* 6: 773-782.

Karihaloo, B.L. 1995. *Fracture Mechanics and Structural Concrete*. UK: Addison Wesley Longman.

Karihaloo, B.L. 1999. Size effect in shallow and deep notched quasi-brittle structures. *Int J Fract* 95: 379-390.

Karihaloo, B.L., Abdalla, H.M. & Imjai, T. 2003a. A simple method for determining the true specific fracture energy of concrete. *Mag Concr Res* 55: 471-481

Karihaloo, B.L., Abdalla, H.M. & Xiao, Q.Z. 2003b. Size effect in concrete beams. *Engng Fract Mech* 70: 979-993.

Karihaloo, B.L. & Xiao, Q.Z. 2001. Higher order terms of the crack tip asymptotic field for a notched three-point bend beam. *Int J Fract* 112: 111-128.

Olesen, J.F. 2001. Fictitious crack propagation in fiber-reinforced concrete beams. *ASCE J of Engng Mech* 127: 272-280.

Planas, J., Bazant, Z.P. & Jirasek, M. 2001. Reinterpretation of Karihaloo's size effect analysis for notched quasibrittle structures. *Int J Fract* 111: 17-29.

Roelfstra, P.E. & Wittmann, F.H. 1986. Numerical method to link strain softening with failure of concrete. In F.H. Wittmann (ed.), *Fracture Toughness and Fracture Energy of Concrete*: 163-175. Amsterdam: Elsevier.

Ulfkjaer, J.P., Krenk, S. & Brincker, R. 1995. Analytical model for fictitious crack propagation in concrete beams. *ASCE J Engng Mech* 121: 7-15.

Van Vliet, M.R.A. & Van Mier, J.G.M. 1999. Effect of strain gradients on the size effect of concrete in uniaxial tension. *Int J Fract* 95: 195-219.

Xiao, Q.Z. & Karihaloo, B.L. 2002. Approximate weight functions for singular and higher order terms of an edge crack in a finite plate. *Engng Fract Mech* 69:959-978.

Zech, B. & Wittmann, F.H. 1978. A complex study on the reliability assessment of the containment of PWR. Part II: Probabilistic approach to describe the behaviour of materials. *Nucl Engng Des* 48: 563-593.